Kinetic Control of Catalytic CVD for High-Quality Graphene at Low Temperatures

Robert S. Weatherup, Bruno Dlubak, and Stephan Hofmann*

Department of Engineering, University of Cambridge, Cambridge CB3 0FA, U.K.

ABSTRACT

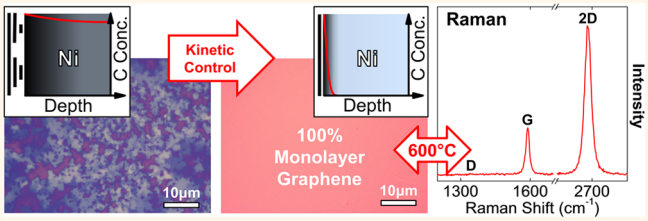

Low-temperature (~600 °C), scalable chemical vapor deposition of high-quality, uniform monolayer graphene is demonstrated with a mapped Raman 2D/G ratio of >3.2, D/G ratio ≤0.08, and carrier mobilities of ≥3000 $cm^2 V^{-1} s^{-1}$ on SiO_2 support. A kinetic growth model for graphene CVD based on flux balances is established, which is well supported by a systematic study of Ni-based polycrystalline catalysts. A finite carbon solubility of the catalyst is thereby a key advantage, as it allows the catalyst bulk to act as a mediating carbon sink while optimized graphene growth occurs by only locally saturating the catalyst surface with carbon. This also enables a route to the controlled formation of Bernal stacked bi- and few-layered graphene. The model is relevant to all catalyst materials and can readily serve as a general process rationale for optimized graphene CVD.

KEYWORDS: graphene · chemical vapor deposition · low temperature · catalyst · Ni · bilayer · Bernal stacking

Chemical vapor deposition (CVD) is the most promising route toward scalable graphene production and integration, key requirements for the commercial exploitation of graphene's unique properties. While progress has been made in achieving graphene CVD over large areas,[1−3] the underlying growth mechanisms have yet to be fully understood to enable further process optimization. A key aspect of the CVD process is the choice of catalyst. Cu is currently the most widely used catalyst material, as it allows a rather error-tolerant window for the formation of monolayer graphene (MLG) on its surface at high temperatures (>900 °C). The prevalent rationale for catalyst choice is thereby based on the carbon solubility: a low carbon solubility, such as for Cu, is thought to be preferable to prevent carbon dissolution and a bulk reservoir effect that would make it difficult to get uniform graphene due to carbon precipitation upon cool-down.[4] For high-temperature (>800 °C) CVD with catalysts of higher carbon solubility, such as Ni, it is indeed very challenging to achieve graphene uniformity and layer control.[5−7] It should be noted, however, that, in contrast to Cu, Ni is a much better catalyst for (1) the dissociation of typically used carbon precursors and (2) the formation of a graphitic lattice. Hence Ni can enable a significant reduction in process temperature while maintaining the same graphene quality;[7] that is, Ni should be a catalyst material of choice for low-temperature CVD. This is further motivated by surface science studies exposing Ni(111) single crystals, that highlight MLG formation at <750 °C and the theoretically almost perfect lattice match between Ni(111) and MLG.[8,9]

Here we report scalable graphene CVD on Ni-based catalysts at ~600 °C with complete monolayer coverage as well as layer control and show that it is actually possible to achieve a uniformity and quality that has hitherto only been reported for Cu-based CVD at ~1000 °C.[2,3,10] We show that the finite carbon solubility of the catalyst bulk is thereby actually a key advantage, in contrast to previous literature, which always saw it as undesirable.[4] We introduce a relatively simple kinetic growth model that not only shows excellent agreement with our systematic experimental study but, we think, is of general relevance to all catalyst materials and optimized graphene CVD.

RESULTS AND DISCUSSION

Figure 1 shows the uniformity and quality of MLG achieved by low-temperature (~600 °C) CVD on a Au(10 nm)-decorated Ni foil (25 μm thickness). A simple one-step CVD process is used, whereby the samples are

* Address correspondence to sh315@cam.ac.uk.

Received for review August 13, 2012 and accepted October 1, 2012.

Published online October 01, 2012
10.1021/nn303674g

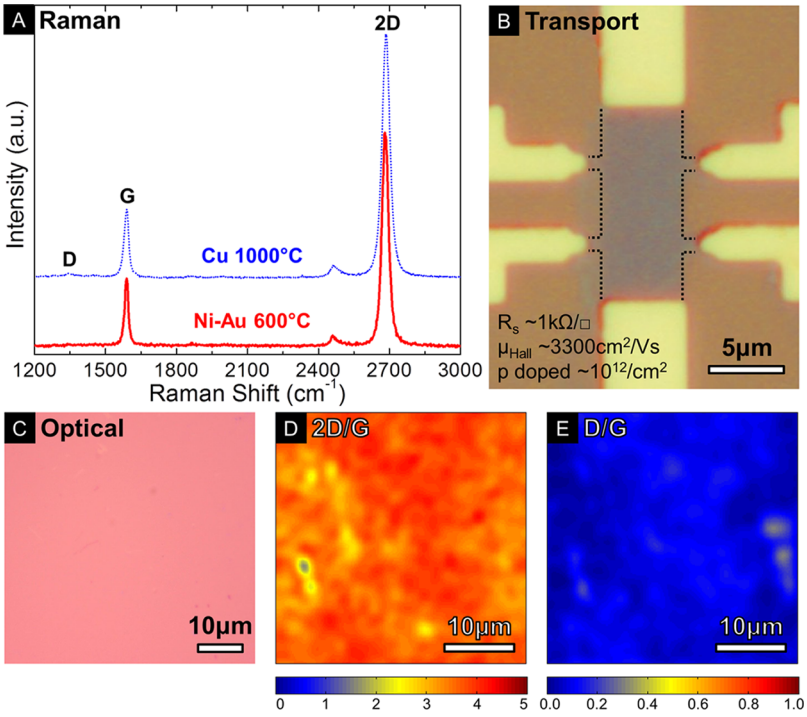

Figure 1. (A) Raman spectrum of MLG grown on Au(10 nm)/Ni(25 μm) by C_6H_6 (10^{-3} m bar) exposure for 30 min at ~600 °C and subsequently transferred to Si/SiO_2(300 nm) using the bubbling transfer method and a reference spectrum of MLG grown on Cu by CH_4 exposure at 1000 °C from Kidambi *et al.*[10] (B) Optical micrograph of Hall bar device fabricated from the transferred MLG grown on Au(10 nm)/Ni(25 μm) using e-beam lithography, O_2 plasma etching, and thermally evaporated Ti/Au contacts. (C) Optical micrograph of as-transferred MLG grown on Au(10 nm)/Ni(25 μm). (D, E) Corresponding Raman maps of 2D/G peak intensity (D) and D/G peak intensity (E).

heated in H_2, exposed to an undiluted hydrocarbon, and then cooled in vacuum (see Methods). We note that the Raman and transport measurements are performed after MLG transfer to SiO_2(300 nm)-covered Si wafers, *i.e.*, include possible degradation incurred during transfer. Figure 1A shows a typical Raman spectrum for our CVD MLG, with a 2D/G ratio of ~3.2 and a 2D peak (~2680 cm^{-1}) that is well fitted by a single Lorentzian with a fwhm of ~31 cm^{-1}. The D peak (~1340 cm^{-1}) is very small and almost undetectable above the measurement background, suggesting a very low defect density. Little difference is seen compared to a Raman spectrum representative of Cu-catalyzed MLG at 1000 °C.[10] Figure 1B–D show an optical image of the same low-temperature MLG as well as 35 × 35 μm Raman maps of measured 2D/G and D/G intensity ratios. The mapped region has an average 2D/G ratio of ~3.4 with >99.9% of the area having a 2D/G ratio >2 (Figure 1D). The average D/G ratio is ~0.08, significantly lower compared to recent literature, where D/G ratios as high as 0.85 are reported for similar growth temperatures of 600 °C.[11] Six contact Hall-geometry devices based on our low-temperature CVD MLG (Figure 1B) give mobilities (on SiO_2 support) ≥ 3000 $cm^2\ V^{-1}\ s^{-1}$ (with a p doping of ~10^{12} cm^{-2}), equaling the mobilities we measure for high-temperature Cu-catalyzed MLG[10] and an order of magnitude larger than for previously reported low-temperature growth at 600 °C.[11] We note that the measured mobilities are likely to be limited by extrinsic factors such as impurities introduced by the transfer process, adsorbates from the atmosphere, and support interactions.[12,13]

Figure 2 schematically highlights the key points of our kinetic growth model, central to understanding why such high quality and layer control is feasible with Ni-based catalysts at low temperatures. We note that previous literature has typically treated the catalyst bulk as an undesirable reservoir and thereby generally neglected any kinetic effects during exposure.[4] Figure 2A shows the carbon fluxes essential to graphene CVD, involving precursor dissociation (process 1) and the formation of graphitic layers (process 2). In modeling process 1 we wish to determine the flux of dissociated carbon reaching the catalyst surface, J_S, based on the impingement flux of carbon from the precursor, J_I. J_S will vary with the areal graphene coverage,[14,15] while J_I, when modeled within the widely used kinetic theory of gases, will be constant for a given precursor, exposure pressure, and temperature. Here we assume that each graphene layer is not a perfectly impermeable layer but allows a certain proportion, p, of the carbon flux to pass through. J_S can therefore be calculated on the basis of the fractional area coverage, θ_n, of the currently growing nth graphene layer and the carbon flux reaching the catalyst surface through these n layers, $p^n J_I$, and the carbon flux through the $(n-1)$

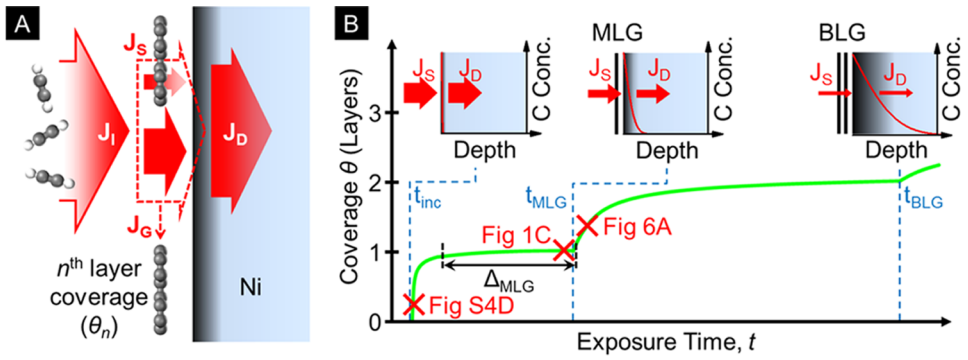

Figure 2. (A) Schematic showing the relationship between the significant carbon fluxes accounted for in the graphene growth model. The carbon fluxes associated with the precursor impingement, J_I, dissociation at the catalyst surface, J_S, diffusion into the catalyst, J_D, and graphene formation, J_G, are considered. (B) Schematic indicating how graphene coverage evolves for a semi-infinite catalyst based on the growth model developed, with insets indicating the carbon concentration throughout the catalyst film at various stages of the growth. Red crosses indicate the approximate stages of growth that Figures S4D, 1C, and 6A correspond to.

layers that cover the remaining area, $p^{(n-1)}J_I$, which gives

$$J_S = \theta_n p^n J_I + (1 - \theta_n) p^{(n-1)} J_I \quad (1)$$

We assume thereby that multilayer graphene grows isothermally during exposure to the carbon precursor[7] and sequentially in contact with the metal catalyst; that is, a new layer nucleates below a complete surface coverage of the preceding layer.[16] These assumptions will be justified below. We note that exfoliated graphene flakes have been shown to be impermeable to gases,[17] but the carbon leakage can be attributed to the inherent polycrystallinity of CVD graphene whereby the domain boundaries and other defects offer pathways for carbon to reach the catalyst.

In process 2, the difference between J_S and the diffusive flux of carbon from the surface into the catalyst, J_D, yields the flux of carbon that feeds the growing graphene layer, J_G. J_D can be obtained by consideration of 1D Fickian diffusion perpendicular to the catalyst surface (see Supporting Information). The catalyst is thereby assumed to have an initially uniform carbon concentration, c_0, throughout its thickness, and the carbon diffusivity in Ni, D, is taken to only vary with temperature and thus is held constant during the isothermal precursor exposure. For simplicity, we account here only for spatial variations perpendicular to the catalyst surface. Figure 2B illustrates how the calculated graphene coverage θ develops during precursor exposure and at the same time indicates the carbon distribution in the Ni catalyst at salient stages of the growth. At the start of carbon precursor exposure there is an incubation period in which J_S is matched by J_D, meaning θ remains at zero, but the carbon concentration at the Ni catalyst surface, c_{surf}, gradually increases. For a Ni catalyst of infinite thickness, the variation in c_{surf} with time, t, after introducing the carbon precursor is given by

$$c_{surf}(t) = c_0 + 2J_I\sqrt{\frac{t}{\pi D}} \quad (2)$$

Nucleation of graphene occurs when a certain carbon concentration, c_{nuc}, at the Ni surface is reached, which is supported by our previous observations of a notable incubation time and an interstitial carbon-based expansion of the Ni lattice.[7,15] The incubation time, t_{inc}, is given by

$$t_{inc} = \frac{\pi D}{4}\left(\frac{c_{nuc} - c_0}{J_I}\right)^2 \quad (3)$$

For realistic catalyst films, we consider individual grains that extend throughout the entire catalyst thickness, l, with the back side not exposed. Equation 1 can be adjusted for this (see Supporting Information), and a lower limit for t_{inc} is approached for low J_I (with respect to catalyst thickness), where slow filling of the catalyst results in a more uniform distribution of carbon throughout the thickness:

$$t_{inc} \rightarrow \frac{(c_{nuc} - c_0)l}{J_I} \quad (4)$$

After nucleation, c_{surf} is modeled as being held constant at the Ni solubility limit, S, which results in $J_S > J_D$ (*i.e.*, $J_G > 0$), and growth proceeds as schematically indicated in Figure 2B. There is a rapid rise in θ following the nucleation of a new graphene layer, as the uncovered area, $(1 - \theta_n)$, is initially large and thus J_S is initially high. The growth rate diminishes as θ_n increases, and there is a notable plateau in θ_n prior to the nucleation of the next layer. Here we define this plateau as when >95% coverage of the respective graphene layer is achieved, as shown for the MLG plateau, Δ_{MLG}, in Figure 2B. The next layer nucleates only when c_{nuc} is reached at the catalyst surface and grows when J_S exceeds J_D, *i.e.*, when the gradient of carbon concentration close to the catalyst

surface reaches J_D/D, as shown by the inset schematics of the concentration profiles in Figure 2B.

Realistic metal catalysts for scalable graphene CVD are polycrystalline, and this will lead to variations in D perpendicular to the surface, as well as variations in the precursor sticking coefficient (and thus J_S), and c_{nuc} for different Ni grain orientations. These variations ultimately mean that for different Ni grains it will take different times to reach complete coverage. Therefore for a robust MLG growth process, in which uniform coverage over many different catalyst grain orientations can be achieved, a large value of Δ_{MLG} with respect to t_{inc} is desired. We therefore refer to Δ_{MLG}/t_{inc} as a robustness parameter for MLG growth, and we note that Δ_{MLG}/t_{inc} is increased by reducing the leakage, p, or increasing the nucleation barrier for the next layer, c_{nuc}.

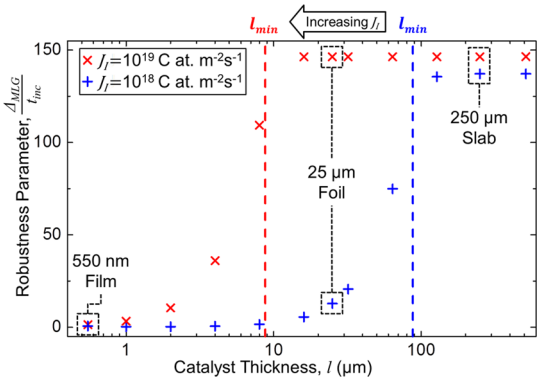

Figure 3. Calculated relationship between catalyst thicknesses and the MLG formation robustness parameter (the ratio between MLG plateau width and incubation time, Δ_{MLG}/t_{inc}) for different carbon impingement fluxes (J_I). A larger value of Δ_{MLG}/t_{inc} indicates a more robust process for MLG formation over large areas. Data points corresponding to the conditions used in our experimental study are labeled. The lower bounds for the catalyst thickness required to avoid saturating the catalyst throughout its thickness during MLG formation (l_{min}) are also indicated for the different values of J_I. The data are obtained using the kinetic model presented and are implemented using a finite-difference Crank–Nicolson method (see Supporting Information) with the value of p fixed at 0.05 and values of S and D calculated for a growth temperature of 600 °C, based on the results of Lander *et al.*[29]

We implement our model using a finite-difference Crank–Nicolson method[18] to calculate the variation of θ with t (see Supporting Information), and Figure 3 shows the extracted robustness parameters (Δ_{MLG}/t_{inc}) for different values of J_I and l. This reveals some key trends in particular regarding exposure conditions and optimum catalyst thickness. Assuming for instance $J_I = 10^{18}$ C atoms m^{-2} s^{-1}, the 550 nm and 25 μm thick catalyst films become saturated with carbon throughout their thickness before complete MLG coverage is achieved, and so Δ_{MLG}/t_{inc} is low; that is, no robust MLG growth can be expected. On the other hand, a higher J_I value of 10^{19} C atoms m^{-2} s^{-1} results in both the 25 and 250 μm thick catalyst films being saturated only near the catalyst surface during MLG CVD, and the corresponding large value of Δ_{MLG}/t_{inc} suggests that robust MLG formation should be possible.

This clearly highlights a distinct difference in growth behavior between a catalyst saturated with carbon throughout its thickness and one that is saturated only near the exposed surface. In the latter case, diffusion from the catalyst surface into the bulk mediates graphene growth and hence gives a broad processing window to achieve layer control by CVD. A lower bound for the catalyst thickness required to grow n layers of graphene without saturating the bulk throughout its thickness, l_{min}, is given by

$$l_{min} = \frac{DS}{p^n J_I} \quad (5)$$

We note that for increasing values of n the carbon flux to the Ni surface is rapidly reduced, and so for conditions similar to those used herein, n will be limited in practice to less than 3–4 layers for realistic exposures. On the basis of eq 5, the lower thickness bound for MLG formation has been plotted in Figure 3 for the different values of J_I, and it corresponds extremely well with the low to high transition of the robustness parameter.

Whether inhomogeneous few-layer graphene (FLG) is formed is determined by p and the extent to which the Ni bulk is saturated with carbon during growth. If p is high, additional layers will be easily formed by

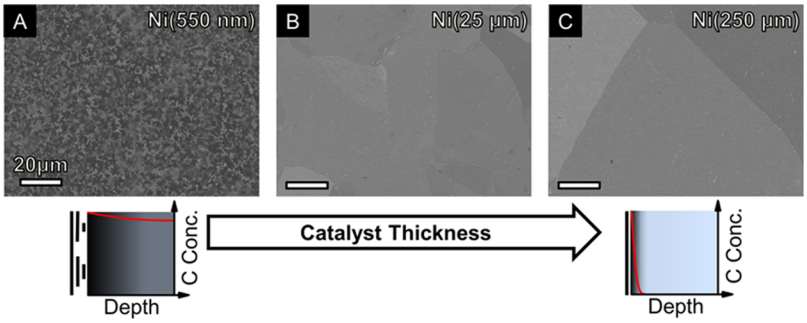

Figure 4. SEM micrographs of elemental Ni catalyst surfaces following C_2H_2 (10^{-5} mbar) exposures at ~600 °C for 15 min for Ni catalyst thicknesses of 550 nm (A), 25 μm (B), and 250 μm (C). All scale bars are 20 μm.

carbon diffusing through existing graphene layers, whereas even a modest carbon flux through existing graphene will result in the formation of additional graphene layers if the bulk of the catalyst is already well saturated with carbon.

Our model highlights that for controlled graphene CVD it is highly advantageous to tune conditions for the catalyst bulk not to be fully saturated with carbon. This directly relates to an optimum catalyst thickness for given CVD conditions or *vice versa*. We corroborate our model *via* a systematic growth study of Ni-based graphene CVD in particular looking at Ni catalyst thickness, exposure time, and exposure pressure. As a reference, we use exposures of Ni(25 μm) foils to C_2H_2 at 10^{-5} mbar for 15 min. Figure 4A–C show that varying the Ni thickness has a significant impact on the growth outcome. The Ni(25 μm) foil and Ni(250 μm) slab show uniform MLG coverage across different Ni grains. This corresponds closely to the thicknesses at which robust MLG formation is expected with a J_I value of 10^{19} C atoms m^{-2} s^{-1} (as shown in Figure 3), where l_{min} is ~9 μm. In contrast the Ni(~550 nm) film shows highly inhomogeneous multilayer graphene formation for the same CVD conditions. The typical size of each region of constant contrast for the Ni(~550 nm) film in Figure 4A is on the same order as the Ni grain size in these films (<1 μm), indicating that the multilayer graphene coverage is strongly dependent on the underlying Ni grain structure. The fact that for the given CVD conditions only the thicker Ni gives homogeneous MLG is consistent with our kinetic model, which predicts the thin Ni to be saturated with carbon, while for the thicker Ni, diffusion into the catalyst bulk mediates the growth of MLG and hence gives robust process conditions.

The carbon diffusion flux into the catalyst bulk, J_D, is crucial in providing a mediating balance (Figure 2), but as a result a notable portion of the carbon dissociated at the catalyst surface dissolves into the catalyst bulk. It is important to note that under the described optimized conditions this carbon does not precipitate upon cooling but remains in the catalyst. Figure 5A shows direct evidence for this, whereby after exposing a Ni(250 μm) slab to reference conditions (Figure 4C) we removed as-grown MLG and dissolved the Ni to reveal a gray translucent film of amorphous carbon, as confirmed by Raman spectroscopy (see Figure 5A inset). In comparison, Figure 5B shows the residual film left for a Ni(250 μm) slab exposed at a lower C_2H_2 exposure pressure (10^{-6} mbar, 240 min), which appears much darker and is almost completely opaque. This confirms that for the reference conditions the catalyst is not fully saturated with carbon and that conditions corresponding to a reduction in J_I result in a more carbon-saturated catalyst bulk during growth, as predicted by our kinetic model. We note that for standard transfer techniques this dissolved carbon

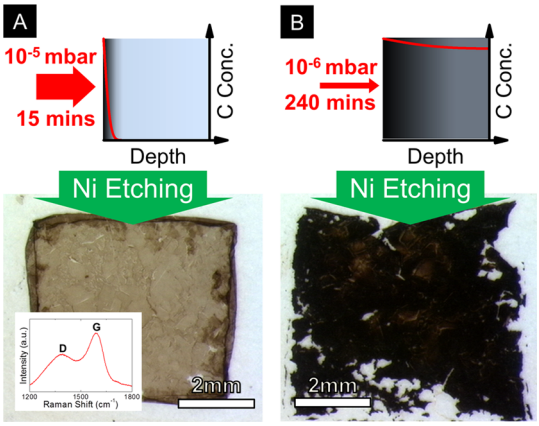

Figure 5. Optical micrographs of residual material following removal of as-grown MLG by bubbling transfer and subsequent Ni removal by etching with a 1 M $FeCl_3$ aqueous solution for Ni(250 μm) slabs exposed to (A) C_2H_2 (10^{-5} mbar) for 15 min at ~600 °C [inset with corresponding Raman spectrum] and (B) C_2H_2 (10^{-6} mbar) for 240 min at ~600 °C. All scale bars are 2 mm. Sketches representative of the different extent of carbon filling of the catalysts are also shown.

may also be transferred and hence lead to contamination. This motivates the bubbling-based transfer used here.[19,20] We also performed postannealing experiments (600 °C, 45 min under vacuum) on as-grown samples following a reference C_2H_2 exposure, prior to cooling (see Supporting Information). This resulted in the almost complete disappearance of the MLG from the Ni(250 μm) slab, which we attribute to carbon dissolution into the catalyst bulk, corresponding to a reduction in the carbon concentration near the catalyst surface as the carbon distribution homogenizes throughout the Ni thickness. For the Ni(25 μm) foil and Ni(550 nm) film the graphene coverage remains unchanged for the postannealing, indicating the average carbon concentration throughout the catalyst is higher (as the catalyst is thinner) and thus the surface carbon concentration is not reduced adequately during annealing for the graphene to be dissolved. We therefore note that the thermal stability of graphene on Ni depends on the carbon concentration close to the catalyst surface and not simply temperature.[9]

Figure 2 highlights the carbon flux balance, and as shown in Figure 3, the precursor impingement flux J_I thereby sets the boundary conditions. For a simple ideal gas approximation, J_I is directly proportional to the carbon precursor partial pressure. For a CVD reactor, this will be more complex dependent for instance on the gas flow regime. Many reactors tend to operate in a transitional or viscous flow regime, where precursor diffusion through a gas boundary layer can be rate limiting. Our experimental study here focuses on low temperatures and relatively low pressures, for which we expect the CVD process not to be mass-transfer limited, but surface reaction controlled. We observe a clear dependence on carbon precursor pressure (see Supporting Information), fully supporting

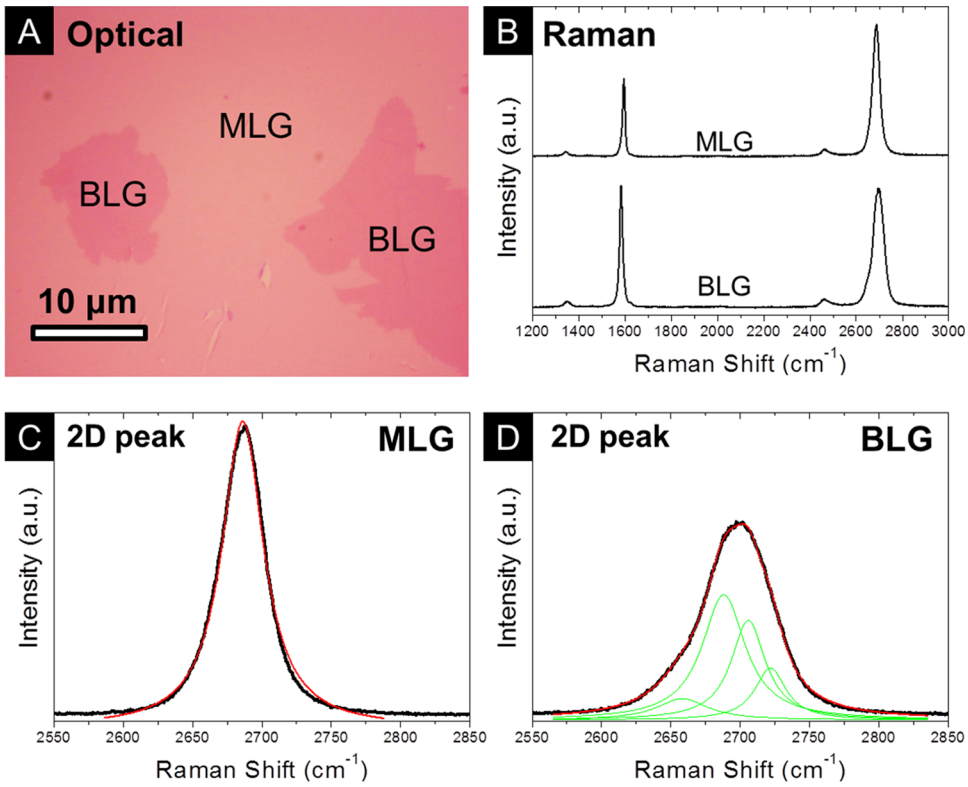

Figure 6. (A) Optical micrograph of M-/BLG grown on Au(25 nm)/Ni(25 μm) by C_2H_2 (10^{-4} mbar) exposure for 30 min at ~600 °C and subsequently transferred to Si/SiO_2(300 nm) using the bubbling transfer method. (B) Raman spectra corresponding to MLG and BLG regions and the respective 2D peaks fitted with a single Lorentzian peak for MLG (C) and four Lorentzians for BLG (D).

the predictions of our kinetic model. In particular, we find that for instance a 10-fold reduction in C_2H_2 pressure relative to our MLG reference conditions, combined with a corresponding increase in exposure time for maintaining the same total catalyst surface exposure, results in inhomogeneous multilayer graphene formation. This corresponds to the implication of our kinetic model that a reduction in J_I, with the catalyst thickness held constant, leads to a more carbon-saturated catalyst bulk during growth (see Figure 5B) and thus a less robust process (see Figure 3). We note that for significantly higher exposure pressures and/or lower growth temperatures than used here additional graphene layers will form prior to the completion of the first layer. Therefore when applying the model presented, the magnitude of J_S in comparison to the carbon diffusivity at the catalyst surface must be considered to determine whether the assumption of layer-by-layer growth remains valid.

Our previous *in situ* studies of graphene formation on Ni-based catalysts have directly shown that graphene is readily formed isothermally on Ni thin films[7] and that the relative contribution of carbon precipitation on cooling can be negligible for growth temperatures of <650 °C.[15] There is also strong evidence that at the conditions used, graphene grows only in direct contact with the catalyst; that is, for multilayer films additional graphene layers grow underneath the already grown graphene coverage.[16] Looking at the exposure dependence of our growth results (see Supporting Information), we find that, for conditions for which complete MLG coverage is achieved, extended exposure times result in the growth of additional graphene layers. This is consistent with the previous *in situ* evidence and also with our model predictions (as outlined in Figure 2B), which capture the carbon leakage through domain boundaries in the covering graphene by the parameter *p*. As previously mentioned, the motivation for the use of Ni is that it is highly catalytically active regarding precursor dissociation. Our systematic *in situ* studies show for instance that at temperatures of around 350 °C, C_2H_2 as well as other precursors such as C_6H_6 readily dissociate on Ni. This clearly shows that there is no motivation and no need for an additional plasma excitation for graphene CVD at such low temperatures, unlike suggested in previous literature.[21,22] Our data herein show that the overall exposure dependence is very similar for C_6H_6 compared to C_2H_2 as precursor. We note that C_2H_2 is the more reactive carbon source, corresponding to carbon supplied at a higher chemical potential. This is reflected in a lower optimum C_2H_2 pressure compared to C_6H_6 (see Supporting Information).

In order to further optimize the CVD process, our experimental study focuses here on increasing the graphene domain sizes, which should lead to a

reduction in the leakage p and a corresponding increase in Δ_{MLG}, giving a more robust process. We previously showed that the graphene nucleation density can be effectively lowered *via* Ni alloying, *e.g.*, with noble metals.[7] We clearly confirm here that also for thick Ni foils the thermal evaporation of a thin Au coating allows a significant reduction in MLG nucleation density with a corresponding increase in the lateral size of the MLG domains from ~1 μm for elemental Ni(25 μm) foils to >20 μm for Au(25 nm)/Ni(25 μm) foils (see Supporting Information). These data also confirm our model predictions, as there is indeed an improvement in the robustness of the process: homogeneous MLG is formed on Au-coated Ni foils after C_2H_2 (10^{-4} mbar) exposures for 15 min, while similar exposures yield inhomogeneous multilayer graphene coverage on elemental Ni foils. This increase in Δ_{MLG} is crucial (see Figure 2B) to achieve uniform graphene coverage over many different catalyst grain orientations.

Figure 2B highlights that beyond homogeneous MLG coverage our model also gives conditions for controlled growth of few-layer graphene. Bilayer graphene (BLG) should grow *via* secondary nucleation under a continuous MLG film for increased exposures times and/or precursor pressures. An adequate carbon flux through the existing MLG is important to achieve this (dependent on p), and therefore using a higher exposure pressure should lead to more rapid formation of a second graphene layer. Figure 6A shows that by increasing the C_2H_2 exposure pressure to 10^{-4} mbar and the exposure time to 30 min, BLG islands ~10 μm in dimension form as predicted in the presence of a complete MLG coverage. This extent of growth approximately corresponds to the position marked in Figure 2B. Figure 6B shows Raman spectra for the MLG and BLG regions, confirming the number of layers and good graphitic quality (D/G ratio of ~0.05). Figure 6C and D show the 2D peaks from these Raman spectra fitted with a single Lorentzian (fwhm of 36 cm^{-1}) in the case of the MLG and with four Lorentzian peaks in the case of BLG, which indicates that the BLG is Bernal stacked.[23] Our approach therefore offers a promising new route to forming Bernal stacked bilayers, for which interesting properties have recently been shown including tunable band gaps.[24]

CONCLUSIONS

In conclusion, we have shown that through appropriate catalyst and process engineering complete coverage of high-quality MLG can be achieved by scalable CVD at ~600 °C. Importantly we demonstrate that continuous, uniform growth is achieved even for polycrystalline catalysts. A finite carbon solubility of the catalyst is thereby a key advantage, as the catalyst bulk acts as a mediating carbon sink that moderates the variations in growth seen for instance for different catalyst grain orientations. Optimized growth is achieved by only locally saturating the catalyst with carbon near the growth surface, which translates into matching the CVD exposure conditions to the catalyst thickness. We note that this diffusion-mediated growth does not necessarily require a thick catalyst film and that a suitable carbon sink could be artificially engineered for example by using catalyst alloys or heterostructures containing high carbon solubility and/or stable carbide-forming elements. In fact several reports have incidentally made use of such structures and observed robust MLG formation,[25,26] although this has previously been attributed to a reduction in precipitation on cooling rather than the diffusion-moderated isothermal growth we show here. We establish a kinetic growth model for graphene CVD based on carbon flux balances, which is well supported by our systematic study of the parameter space of Ni-based catalysts. We thereby also show a route to the controlled formation of Bernal stacked bi- and few-layered graphene. Our results and model are of general relevance to all catalyst materials, in particular highlighting that, contrary to previous literature, a finite carbon solubility is not necessarily a negative attribute. Our model can readily serve as a general process rationale for optimized graphene CVD.

METHODS

We investigate sputter-deposited, polycrystalline Ni films (~550 nm thick, 99.995% purity sputter target) on SiO_2(300 nm)/Si substrates, polycrystalline Ni foils (25 μm thick, Alfa Aesar 99.99% purity), and polycrystalline Ni slabs (250 μm thick, Alfa Aesar 99.994% purity). Au−Ni catalysts are produced by thermal evaporation of Au(0−50 nm) directly on top of the Ni catalyst prior to annealing and growth. The samples are annealed [~600 °C, H_2 (1 mbar) for 15 min, heated at ~300 °C/min], exposed to hydrocarbons [~600 °C, C_2H_2 (10^{-6}−10^{-3} mbar) or C_6H_6 (10^{-4}−10^{-3} mbar)], and then cooled [under vacuum at ~100 °C/min] in a custom-built cold-wall reactor [base pressures 5×10^{-7} mbar]. The annealing stage is found to promote grain growth of the catalyst films and ensure sufficient alloying for the Au−Ni catalysts.

Samples are characterized *ex situ*, either as-grown using scanning electron microscopy (SEM, FEI Philips XL30s/Zeiss SigmaVP, 1 kV) or after transfer of the M-/FLG films to SiO_2-(300 nm)/Si substrates, using optical microscopy and Raman spectroscopy (Renishaw Raman InVia microscope, 532 nm excitation). Regions not covered with graphene appear brighter on average in the SEM micrographs, as a result of the higher secondary electron yield of Ni compared to MLG,[27] while increasingly thick FLG layers appear darker. There are also significant variations in contrast associated with electron channeling contrast arising from the different grain orientations in the underlying polycrystalline Ni foils.[28] These different contrast mechanisms can generally be distinguished by the shape and size of the features they are associated with, which has been further corroborated by M-/FLG transfers to SiO_2(300 nm)/Si

substrates. Transfer is carried out using polymethylmethacrylate (PMMA) to support the M-/FLG films and an electrolysis-based bubbling technique[19,20] with the PMMA/graphene/Ni sample as the cathode and a Pt wire anode in a NaOH (1 M) aqueous solution. Following removal of the catalyst layer, the PMMA-supported M-/FLG films are rinsed in DI water and transferred to SiO_2(300 nm)/Si substrates, and the PMMA is then dissolved away using acetone. This process leaves the catalyst film intact,[19,20] and optical microscopy and low-magnification TEM of the transferred graphene show no significant metal remnants. To isolate the residual carbon left in the intact Ni films, wet etching of the catalyst layer in a $FeCl_3$ (1 M) aqueous solution was used to remove the Ni.

Electrical measurements are performed at room temperature using Hall bar devices fabricated by e-beam lithography on transferred MLG (see Figure 1B). The MLG is patterned by an O_2 plasma etch, and then Ti/Au contacts are evaporated on top.

Conflict of Interest: The authors declare no competing financial interest.

Acknowledgment. R.S.W. acknowledges funding from EPSRC (Doctoral Training Award). S.H. acknowledges funding from ERC grant InsituNANO (no. 279342). This research was partially supported by the EU FP7 Work Programme under grant GRAFOL (project reference 285275).

Supporting Information Available: Description of the derivation of the kinetic model and additional experimental data relating to the systematic growth study of Ni-based polycrystalline catalysts. This material is available free of charge *via* the Internet at http://pubs.acs.org.

REFERENCES AND NOTES

1. Yu, Q.; Lian, J.; Siriponglert, S.; Li, H.; Chen, Y. P.; Pei, S. S. Graphene Segregated on Ni Surfaces and Transferred to Insulators. *Appl. Phys. Lett.* **2008**, *93*, 113103.
2. Li, X.; Cai, W.; An, J.; Kim, S.; Nah, J.; Yang, D.; Piner, R.; Velamakanni, A.; Jung, I.; Tutuc, E.; *et al*. Large-Area Synthesis of High-Quality and Uniform Graphene Films on Copper Foils. *Science* **2009**, *324*, 1312–1314.
3. Bae, S.; Kim, H.; Lee, Y.; Xu, X.; Park, J.-S.; Zheng, Y.; Balakrishnan, J.; Lei, T.; Ri Kim, H.; Song, Y. I.; *et al*. Roll-To-Roll Production of 30-Inch Graphene Films for Transparent Electrodes. *Nat. Nanotechnol.* **2010**, *5*, 574–578.
4. Li, X.; Cai, W.; Colombo, L.; Ruoff, R. S. Evolution of Graphene Growth on Ni and Cu by Carbon Isotope Labeling. *Nano Lett.* **2009**, *9*, 4268–4272.
5. Thiele, S.; Reina, A.; Healey, P.; Kedzierski, J.; Wyatt, P.; Hsu, P.-L.; Keast, C.; Schaefer, J.; Kong, J. Engineering Polycrystalline Ni Films to Improve Thickness Uniformity of the Chemical-Vapor-Deposition-Grown Graphene Films. *Nanotechnology* **2010**, *21*, 015601.
6. Reina, A.; Thiele, S.; Jia, X.; Bhaviripudi, S.; Dresselhaus, M. S.; Schaefer, J. A.; Kong, J. Growth of Large-Area Single- and Bi-Layer Graphene by Controlled Carbon Precipitation on Polycrystalline Ni Surfaces. *Nano Res.* **2009**, *9*, 30–35.
7. Weatherup, R. S.; Bayer, B. C.; Blume, R.; Ducati, C.; Baehtz, C.; Schlögl, R.; Hofmann, S. *In Situ* Characterization of Alloy Catalysts for Low-Temperature Graphene Growth. *Nano Lett.* **2011**, *11*, 4154–60.
8. Eizenberg, M.; Blakely, J. Carbon Monolayer Phase Condensation on Ni (111). *Surf. Sci.* **1979**, *82*, 228–236.
9. Addou, R.; Dahal, A.; Sutter, P.; Batzill, M. Monolayer Graphene Growth on Ni(111) by Low Temperature Chemical Vapor Deposition. *Appl. Phys. Lett.* **2012**, *100*, 021601.
10. Kidambi, P. R.; Ducati, C.; Dlubak, B.; Gardiner, D.; Weatherup, R. S.; Martin, M.-B.; Seneor, P.; Coles, H.; Hofmann, S. The Parameter Space of Graphene CVD on Polycrystalline Cu. *J. Phys. Chem. C* **2012**, DOI: 10.1021/jp303597m.
11. Zhang, B.; Lee, W. H.; Piner, R.; Kholmanov, I.; Wu, Y.; Li, H.; Ji, H.; Ruoff, R. S. Low-Temperature Chemical Vapor Deposition Growth of Graphene from Toluene on Electropolished Copper Foils. *ACS Nano* **2012**, *6*, 2471–2476.
12. Pirkle, A.; Chan, J.; Venugopal, A.; Hinojos, D.; Magnuson, C. W.; McDonnell, S.; Colombo, L.; Vogel, E. M.; Ruoff, R. S.; Wallace, R. M. The Effect of Chemical Residues on the Physical and Electrical Properties of Chemical Vapor Deposited Graphene Transferred to SiO_2. *Appl. Phys. Lett.* **2011**, *99*, 122108.
13. Chan, J.; Venugopal, A.; Pirkle, A.; McDonnell, S.; Hinojos, D.; Magnuson, C. W.; Ruoff, R. S.; Colombo, L.; Wallace, R. M.; Vogel, E. M. Reducing Extrinsic Performance-Limiting Factors in Graphene Grown by Chemical Vapor Deposition. *ACS Nano* **2012**, *6*, 3224–3229.
14. Kikowatz, R.; Flad, K.; Hörz, G. Effects of Carbon and Sulfur on the Decomposition of Hydrocarbons on Nickel. *J. Vac. Sci. Technol., A* **1987**, *5*, 1009–1014.
15. Weatherup, R. S.; Bayer, B. C.; Blume, R.; Baehtz, C.; Kidambi, P. R.; Fouquet, M.; Wirth, C. T.; Schlögl, R.; Hofmann, S. On the Mechanisms of Ni-Catalysed Graphene Chemical Vapour Deposition. *ChemPhysChem* **2012**, *13*, 2544–2549.
16. Nie, S.; Walter, A. L.; Bartelt, N. C.; Starodub, E.; Bostwick, A.; Rotenberg, E.; McCarty, K. F. Growth from Below: Graphene Bilayers on Ir(111). *ACS Nano* **2011**, *5*, 2298–2306.
17. Bunch, J. S.; Verbridge, S. S.; Alden, J. S.; van der Zande, A. M.; Parpia, J. M.; Craighead, H. G.; McEuen, P. L. Impermeable Atomic Membranes from Graphene Sheets. *Nano Lett.* **2008**, *8*, 2458–2462.
18. Crank, J. *The Mathematics of Diffusion*, 2nd ed.; Clarendon Press: Oxford, 1979.
19. Wang, Y.; Zheng, Y.; Xu, X.; Dubuisson, E.; Bao, Q.; Lu, J.; Loh, K. P. Electrochemical Delamination of CVD-Grown Graphene Film: Toward the Recyclable Use of Copper Catalyst. *ACS Nano* **2011**, *5*, 9927–9933.
20. Gao, L.; Ren, W.; Xu, H.; Jin, L.; Wang, Z.; Ma, T.; Ma, L.-P.; Zhang, Z.; Fu, Q.; Peng, L.-M.; *et al*. Repeated Growth and Bubbling Transfer of Graphene with Millimetre-Size Single-Crystal Grains Using Platinum. *Nat. Commun.* **2012**, *3*, 699.
21. Kim, J.; Ishihara, M.; Koga, Y.; Tsugawa, K.; Hasegawa, M.; Iijima, S. Low-Temperature Synthesis of Large-Area Graphene-Based Transparent Conductive Films Using Surface Wave Plasma Chemical Vapor Deposition. *Appl. Phys. Lett.* **2011**, *98*, 091502.
22. Kim, Y.; Song, W.; Lee, S.; Jeon, C.; Jung, W.; Kim, M.; Park, C.-Y. Low-Temperature Synthesis of Graphene on Nickel Foil by Microwave Plasma Chemical Vapor Deposition. *Appl. Phys. Lett.* **2011**, *98*, 263106.
23. Ferrari, A.; Meyer, J.; Scardaci, V.; Casiraghi, C.; Lazzeri, M.; Mauri, F.; Piscanec, S.; Jiang, D.; Novoselov, K.; Roth, S.; *et al*. Raman Spectrum of Graphene and Graphene Layers. *Phys. Rev. Lett.* **2006**, *97*, 187401.
24. Zhang, Y.; Tang, T.-T.; Girit, C.; Hao, Z.; Martin, M. C.; Zettl, A.; Crommie, M. F.; Shen, Y. R.; Wang, F. Direct Observation of a Widely Tunable Bandgap in Bilayer Graphene. *Nature* **2009**, *459*, 820–823.
25. Grüneis, A.; Kummer, K.; Vyalikh, D. V. Dynamics of Graphene Growth on a Metal Surface: a Time-Dependent Photoemission Study. *New J. Phys.* **2009**, *11*, 073050.
26. Dai, B.; Fu, L.; Zou, Z.; Wang, M.; Xu, H.; Wang, S.; Liu, Z. Rational Design of a Binary Metal Alloy for Chemical Vapour Deposition Growth of Uniform Single-Layer Graphene. *Nat. Commun.* **2011**, *2*, 522.
27. Luo, J.; Tian, P.; Pan, C.-T.; Robertson, A. W.; Warner, J. H.; Hill, E. W.; Briggs, G. A. D. Ultralow Secondary Electron Emission of Graphene. *ACS Nano* **2011**, *5*, 1047–1055.
28. Goldstein, J.; Newbury, D. E.; Joy, D. C.; Lyman, C. E.; Echlin, P.; Lifshin, E.; Sawyer, L.; Michael, J. R. *Scanning Electron Microscopy and X-Ray Microanalysis*, 3rd ed.; Kluwer Academic Publishers: New York, 2003.
29. Lander, J. J.; Kern, H. E.; Beach, A. L. Solubility and Diffusion Coefficient of Carbon in Nickel: Reaction Rates of Nickel-Carbon Alloys with Barium Oxide. *J. Appl. Phys.* **1952**, *23*, 1305–1309.